

## AN AUGMENTED PROJECTION METHOD FOR THE INCOMPRESSIBLE NAVIER-STOKES EQUATIONS IN ARBITRARY DOMAINS

JUNSEOK KIM

*Department of Mathematics*  
*103 Multipurpose Science and Technology Building*  
*University of California, Irvine, CA 92697-3875, USA*  
*jskim@math.uci.edu*  
*http://math.uci.edu/~jskim/*

Received 22 June 2004

Accepted 11 February 2005

A Cartesian grid method for computing flows with complex immersed, stationary and moving boundaries is presented in this paper. We introduce an augmented projection method for the numerical solution of the incompressible Navier-Stokes equations in arbitrary domains. In a projection method an intermediate velocity field is calculated from the momentum equations, which is then projected onto the space of divergence-free vector fields. In the proposed augmented projection method, we add one more step, which effectively eliminates spurious velocity field caused by complex immersed moving boundaries. The methodology is validated by comparing it with analytic, previous numerical and experimental results.

*Keywords:* Navier-Stokes equation; arbitrary domain; augmented projection method.

### 1. Introduction

In the applications of mathematical modeling in engineering and medical devices, it is often necessary to solve the incompressible Navier-Stokes (NS) equations in irregular domains [Ye *et al.* (1999)]. In this paper we present an augmented projection method for the incompressible NS equations in a domain with embedded irregular boundaries. The applications targeted with this method are wide-ranging and include fluid-structure interaction, multiphase flows, solidification dynamics, and cell mechanics.

Udaykumar *et al.* [2001] has presented a finite-volume Cartesian method, using local geometry and quadratic interpolation functions to calculate flux across the elements that intersect the immersed boundary. This method does not require the coordinate transformation from Euclidian space to general curvilinear coordinates.

Peskin [1977] developed a method which represents a body within a flow field via a forcing term added to the governing equations. When applied at certain points in the flow, this forcing term simulates the effect of the body on the flow, allowing for the modeling of a boundary of any shape within a Cartesian computational box without the necessity of mapping.

In comparison with the other approaches mentioned above, the advantages of the proposed augmented projection method are (i) simple; (ii) versatile; and (iii) straightforward to extend to three-dimensional space, as well as incorporate parallelization and adaptive mesh refinement. For a simple presentation of basic ideas, we focus on (i) and (ii) here and (iii) is left for future paper.

The contents of this paper are arranged as follows. In Sec. 2, governing equations are given. In Sec. 3, we describe the numerical solution. In Sec. 4, we present numerical experiments to validate our new augmented projection scheme. Section 5 concludes the paper.

## 2. Governing Equations

The motion of an incompressible viscous fluid flow is governed by the following Navier-Stokes and continuity equations:

$$\rho \left( \frac{\partial \mathbf{u}}{\partial t} + \mathbf{u} \cdot \nabla \mathbf{u} \right) = -\nabla p + \mu \Delta \mathbf{u}, \quad (1)$$

$$\nabla \cdot \mathbf{u} = 0, \quad (2)$$

on a domain  $\Omega$ , where  $\rho$  is the mass density,  $\mathbf{u}$  is the velocity field,  $p$  is the pressure, and  $\mu$  is the viscosity. Let us define the following dimensionless forms of the variables:  $\mathbf{x}^* = \mathbf{x}/L_*$ ,  $\mathbf{u}^* = \mathbf{u}/V_*$ , and  $p^* = p/\rho V_*^2$ , where asterisk subscript values are characteristic values of length, velocity, and pressure, respectively. Using these dimensionless values, Eqs. (1) and (2) can be written after dropping the asterisk from the dimensionless variables in resulting equations as:

$$\frac{\partial \mathbf{u}}{\partial t} + \mathbf{u} \cdot \nabla \mathbf{u} = -\nabla p + \frac{1}{Re} \Delta \mathbf{u}, \quad (3)$$

$$\nabla \cdot \mathbf{u} = 0, \quad (4)$$

where  $Re = \rho \mu L_*/V_*$  is the Reynolds number. Typical initial and boundary conditions for Eqs. (3) and (4) include specifying an initial velocity field  $\mathbf{u}$  throughout the domain  $\Omega$  and a boundary condition for  $\mathbf{u}$  on the boundary  $\partial\Omega$ .

## 3. Numerical Procedure

Our strategy for solving the systems (3) and (4) is a fractional step scheme having three parts: First we solve the momentum equation (3) without strictly enforcing the incompressibility constraint (4), second we approximately project the resulting velocity field onto the space of discretely divergence-free vector fields

[Bell *et al.* (1989)], third we project approximately divergence-free vector fields onto divergence-free vector fields.

The numerical solution will be for two spatial dimensions and the extension to three dimensions is straightforward. The computational grid consists of rectangular cells of size  $\Delta x$  and  $\Delta y$ ; these cells  $\Omega_{ij}$  are centered at  $(x_i = (i - 0.5)\Delta x, y_j = (j - 0.5)\Delta y)$ , where  $i = 1, \dots, M$  and  $k = 1, \dots, N$ .  $M$  and  $N$  are the numbers of cells in  $x$ -direction and  $y$ -direction, respectively. For simplicity, let  $h = \Delta x = \Delta y$ . The discrete velocity field  $\mathbf{u}_{ij}^n = (u_{ij}^n, v_{ij}^n)$  is located at cell centers. The pressure  $p_{i+\frac{1}{2},j+\frac{1}{2}}^{n-\frac{1}{2}}$  is located at cell corners. The notation  $\mathbf{u}_{ij}^n$  is used to represent an approximation to  $\mathbf{u}(x_i, y_j, t^n)$ , where  $t^n = n\Delta t$  and  $\Delta t$  is a time step. Likewise,  $p_{i+\frac{1}{2},j+\frac{1}{2}}^{n-\frac{1}{2}}$  is an approximation to  $p(x_{i+\frac{1}{2}}, y_{j+\frac{1}{2}}, t^{n-\frac{1}{2}})$ .

The time-stepping procedure is based on the Crank-Nicholson method. At the beginning of each time step, given  $\mathbf{u}^{n-1}$ ,  $\mathbf{u}^n$ , and  $p^{n-\frac{1}{2}}$ , we want to find  $\mathbf{u}^{n+1}$  and  $p^{n+\frac{1}{2}}$  which solve the following second-order temporal discretization of the equation of motion:

$$\frac{\mathbf{u}^{n+1} - \mathbf{u}^n}{\Delta t} = -\nabla_d p^{n+\frac{1}{2}} + \frac{1}{2Re} \Delta_d (\mathbf{u}^{n+1} + \mathbf{u}^n) - (\mathbf{u} \cdot \nabla_d \mathbf{u})^{n+\frac{1}{2}},$$

where the updated flow field satisfies the incompressibility condition

$$\nabla_d \cdot \mathbf{u}^{n+1} = 0.$$

The outline of the main procedures in one time step is follows:

*Step 1. Define  $\psi = 1$  for fluid domain and  $\psi = 0$  for solid domain.*

*Step 2. Initialize  $\mathbf{u}^0$  to be the divergence-free velocity field.*

*Step 3. Compute  $(\mathbf{u} \cdot \nabla_d \mathbf{u})^{n+\frac{1}{2}}$  by using a second order ENO scheme [Shu and Osher (1989)].*

A well-known projection method [Bell *et al.* (1989)] is used for the flow solver, but we treat the advection terms differently from theirs, where the advection terms are computed using a Godunov procedure. Now, we describe the discretization of the advection terms. The half time value  $\mathbf{u}_{ij}^{n+\frac{1}{2}}$  is calculated using an extrapolation from previous values, i.e.  $\mathbf{u}_{ij}^{n+\frac{1}{2}} = (3\mathbf{u}_{ij}^n - \mathbf{u}_{ij}^{n-1})/2$ . In this section, we suppress the  $n + \frac{1}{2}$  temporal index for clarity of expressions. From these cell centered values we obtain cell edged values by

$$u_{i+\frac{1}{2},j} = \frac{u_{i+1,j} + u_{ij}}{2}, \quad v_{i,j+\frac{1}{2}} = \frac{v_{i,j+1} + v_{ij}}{2}.$$

In general, the normal velocities  $u_{i+\frac{1}{2},j}$  and  $v_{i,j+\frac{1}{2}}$  at the edges are not divergence-free. We apply the MAC projection [Sussman and Puckett (2000)] before constructing the convective derivatives. The equation

$$\Delta_d \phi = \nabla_{MAC} \cdot \mathbf{u} \tag{5}$$

is solved for a cell centered  $\phi$ , where  $\Delta_d\phi$  is the standard five point discretization and

$$\nabla_{MAC} \cdot \mathbf{u}_{ij} = \frac{u_{i+\frac{1}{2},j} - u_{i-\frac{1}{2},j}}{h} + \frac{v_{i,j+\frac{1}{2}} - v_{i,j-\frac{1}{2}}}{h}.$$

The resulting linear system (5) is solved using a multigrid method, specifically, V-cycles with a Gauss-Seidel relaxation. Then the divergence-free normal velocities  $\tilde{u}$  and  $\tilde{v}$  are defined by

$$\tilde{u}_{i+\frac{1}{2},j} = u_{i+\frac{1}{2},j} - \frac{\phi_{i+1,j} - \phi_{ij}}{h}, \quad \tilde{v}_{i,j+\frac{1}{2}} = v_{i,j+\frac{1}{2}} - \frac{\phi_{i,j+1} - \phi_{ij}}{h}.$$

From these cell edged values we obtain cell centered values by

$$\tilde{u}_{ij} = \frac{\tilde{u}_{i-\frac{1}{2},j} + \tilde{u}_{i+\frac{1}{2},j}}{2}, \quad \tilde{v}_{ij} = \frac{\tilde{v}_{i,j-\frac{1}{2}} + \tilde{v}_{i,j+\frac{1}{2}}}{2}.$$

The convective term is discretized as:

$$(\mathbf{u} \cdot \nabla_d \mathbf{u})_{ij} = \frac{\tilde{u}_{ij}}{h} (\bar{\mathbf{u}}_{i+\frac{1}{2},j} - \bar{\mathbf{u}}_{i-\frac{1}{2},j}) + \frac{\tilde{v}_{ij}}{h} (\bar{\mathbf{u}}_{i,j+\frac{1}{2}} - \bar{\mathbf{u}}_{i,j-\frac{1}{2}}).$$

The edge values  $\bar{\mathbf{u}}_{i\pm\frac{1}{2},j}$  and  $\bar{\mathbf{u}}_{i,j\pm\frac{1}{2}}$  are computed using a higher order ENO procedure derived in [Shu and Osher (1989)]. The procedure for computing the quantity  $\bar{u}_{i+\frac{1}{2},j}$  is as follows:

$$k = \begin{cases} i & \tilde{u}_{i+\frac{1}{2},j} \geq 0 \\ i+1 & \text{otherwise} \end{cases}$$

$$a = \frac{\tilde{u}_{kj} - \tilde{u}_{k-1,j}}{h}, \quad b = \frac{\tilde{u}_{k+1,j} - \tilde{u}_{kj}}{h}, \quad d = \begin{cases} a & \text{if } |a| \leq |b| \\ b & \text{otherwise} \end{cases}$$

$$\bar{u}_{i+\frac{1}{2},j} = \tilde{u}_{kj} + \frac{h}{2}d(1 - 2(k - i)).$$

The other quantities are computed in the same manner.

Step 4. We solve

$$\frac{\mathbf{u}^* - \mathbf{u}^n}{\Delta t} = -\nabla_d p^{n-\frac{1}{2}} + \frac{1}{2Re} \Delta_d (\mathbf{u}^* + \mathbf{u}^n) - (\mathbf{u} \cdot \nabla_d \mathbf{u})^{n+\frac{1}{2}} \tag{6}$$

using a multigrid method for the intermediate velocity  $\mathbf{u}^*$  without strictly enforcing the incompressibility constraint. Let us rewrite Eq. (6) as

$$\mathbf{u}^* - \frac{\Delta t}{2Re} \Delta_d \mathbf{u}^* = \mathbf{u}^n - \Delta t \nabla_d p^{n-\frac{1}{2}} - \Delta t (\mathbf{u} \cdot \nabla_d \mathbf{u})^{n+\frac{1}{2}} + \frac{\Delta t}{2Re} \Delta_d \mathbf{u}^n, \tag{7}$$

where

$$\nabla_d p_{ij} = \left( \frac{p_{i+\frac{1}{2},j+\frac{1}{2}} + p_{i+\frac{1}{2},j-\frac{1}{2}} - p_{i-\frac{1}{2},j+\frac{1}{2}} - p_{i-\frac{1}{2},j-\frac{1}{2}}}{2h}, \right. \\ \left. - \frac{p_{i+\frac{1}{2},j+\frac{1}{2}} + p_{i-\frac{1}{2},j+\frac{1}{2}} - p_{i+\frac{1}{2},j-\frac{1}{2}} - p_{i-\frac{1}{2},j-\frac{1}{2}}}{2h} \right)$$

and let the right hand side of Eq. (7) be  $(s_1^n, s_2^n)$ . Then we have

$$\mathbf{u}^* - \frac{\Delta t}{2Re} \Delta_d \mathbf{u}^* = (s_1^n, s_2^n). \tag{8}$$

The first component of the Eq. (8) is discretized as follow:

$$\left( 1 + \frac{2\Delta t}{h^2 Re} \right) u_{ij}^* = s_{1ij}^n + \frac{\Delta t}{2h^2 Re} (u_{i+1,j}^* + u_{i-1,j}^* + u_{i,j+1}^* + u_{i,j-1}^*).$$

The second component of Eq. (8) is discretized in a similar manner. The resulting discrete equations are solved using a multigrid method with Gauss-Seidel relaxation.

*Step 5. Project  $\mathbf{u}^*$  onto the space of approximately discrete divergence-free vector fields and get the velocity  $\mathbf{u}^{**}$ , i.e.*

$$\mathbf{u}^* = \mathbf{u}^{**} + \Delta t \nabla_d \phi,$$

where  $\phi$  satisfies  $\Delta_d \phi = \nabla_d \cdot \left( \frac{\mathbf{u}^* - \mathbf{u}^n}{\Delta t} \right)$ . A detailed description of the approximate projection is given by [Almgren *et al.* (1996)]. And then we reset the velocity field by  $\mathbf{u}^{**} = \psi \mathbf{u}^{**}$ .

*Step 6. Update the pressure field,  $p^{n+\frac{1}{2}} = p^{n-\frac{1}{2}} + \phi$ .*

*Step 7. (Augmented projection step).* Since  $\mathbf{u}^{**}$  is an approximately divergence velocity field, we project  $\mathbf{u}^{**}$  into divergence free space using the same procedure in the *Step 3*. And then we reset the velocity field by  $\mathbf{u}^{n+1} = \psi \mathbf{u}^{n+1}$ . These complete one space and temporal step.

### 4. Numerical Results

The proposed augmented projection method for the incompressible NS equations in arbitrary domains has been applied on test problems to verify the accuracy and feasibility of the model. The numerical experiments are the second order convergence in spatial and temporal spaces, simulation of the vortex shedding flow past a cylinder, and simulation of moving boundaries with two-dimensional dendrite growths. We also present a room ventilation simulation, which is quite useful for industrial applications.

#### 4.1. Convergence test

In this section, we validate our scheme by verifying the second-order temporal and spatial convergence. To test our algorithm and obtain an estimate of the rate of

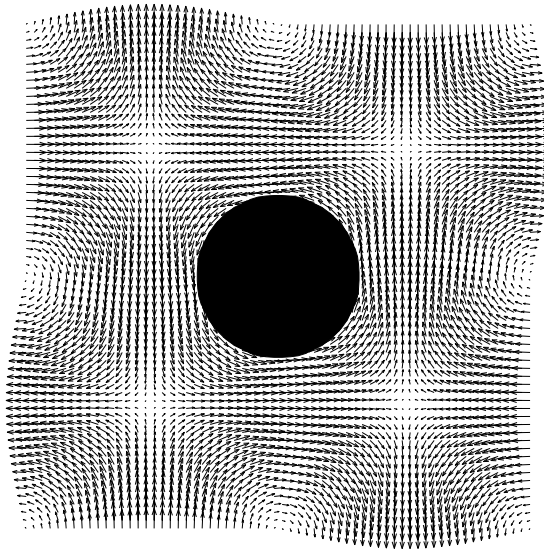


Fig. 1. Geometry and velocity field.

convergence, we perform a number of simulations for a sample initial problem on a set of increasingly finer grids. We take a similar test problem performed in [Tau (1994)].

We apply our algorithm to a domain with one disk (10) (see Fig. 1) which is bounded by a  $2\pi \times 2\pi$  square. We solve the following two-dimensional unsteady flow test problem with known solutions for Eqs. (3) and (4).

$$\begin{aligned} \mathbf{u}(x, y, t) &= (-\cos x \sin y, \sin x \cos y)e^{-\frac{2t}{Re}}, \\ p(x, y, t) &= -\frac{1}{4}(\cos 2x + \cos 2y)e^{-\frac{4t}{Re}}. \end{aligned} \tag{9}$$

$$\psi(x, y) = \begin{cases} 0 & \text{if } \sqrt{(x - \pi)^2 + (y - \pi)^2} < 1 \\ 1 & \text{otherwise} \end{cases}. \tag{10}$$

Exact velocity field  $\mathbf{u}$  (9) on the disk domain ( $\psi \equiv 0$ ) is assumed at each time  $t$ .

The numerical solutions are computed on the uniform grids,  $h = \Delta x = \Delta y = \pi/2^n$  for  $n = 4, 5, 6$  and  $7$ . For each case, the convergence is measured at time  $t = 0.1$  and the uniform time steps,  $\Delta t = 0.1h$ , are used. We define the error to be the discrete maximum norm of the difference between the numerical solution and the exact one:

$$e_h(u) = \max_{ij} |e_{h_{ij}}(u)|, \quad \text{where } e_{h_{ij}}(u) \stackrel{def}{=} u(x_i, y_j) - u_{h_{ij}}.$$

The error of velocity field is measured by  $e_h(\mathbf{u}) = \max(e_h(u), e_h(v))$ . The rate of convergence is defined as the ratio of successive errors:  $\log_2[e_h(\mathbf{u})/e_{\frac{h}{2}}(\mathbf{u})]$ . The errors

Table 1.  $l_2$ -norm of the errors and convergence rates.

$Re$	$32 \times 32$	rate	$64 \times 64$	rate	$128 \times 128$	rate	$256 \times 256$
1	1.82e-3	3.05	2.19e-4	3.21	2.37e-5	3.72	1.18e-6
100	3.04e-3	2.65	4.84e-4	2.53	8.38e-5	2.39	1.60e-5

and rates of convergence for the two  $Re$  numbers ( $Re = 1, 100$ ) are given in Table 1. The results suggest that the numerical scheme is indeed second order accurate.

#### 4.2. Stationary boundary — Vortex shedding flow past a circular cylinder at a Reynolds number of 100

In this section, the Strouhal number, calculated for an immersed cylinder, is compared with previous experimental and numerical results. A large number of experimental and numerical studies have been carried out on the vortex shedding flow that is produced by the flow across a fixed circular cylinder [Strykowski and Sreenivasan 1990]. Depending on the Reynolds number, different kind of flow behaviors can be characterized. At a low Reynolds number, the flow is viscosity dominated. At higher Reynolds number (up to  $Re = 45$ ), two symmetrical standing vortices are formed and attached behind the cylinder. When the Reynolds number gets higher, these vortices develop an altering vortex shedding called the Kármán vortex street. This flow has been previously computed by Johnson and Patel [1999], who used a body fitted grid, and Fadlun *et al.* [2000], who employed variants of hybrid Cartesian/immersed boundary techniques. The present model was tested by simulating flow past a circular cylinder for  $Re = 100$ . The computational domain is  $[0, 32] \times [0, 8]$ . The inflow velocity at the left boundary has a constant value of  $\mathbf{u} = (u_\infty, 0) = (1, 0)$ ; the disk measure  $D = 1$  in diameter and its center is situated at  $(7, 4)$ . The numbers of grid points are  $512 \times 128$  in the streamwise ( $x$ ) and transverse ( $y$ ) directions, respectively. The velocity components of the cylinder,  $\mathbf{u}$ , were set to zero.

$$\psi(x, y) = \begin{cases} 0 & \text{if } \sqrt{(x - 7)^2 + (y - 4)^2} < 1 \\ 1 & \text{otherwise} \end{cases} . \tag{11}$$

For initial data we choose  $u(x, y) = \psi(x, y)$  and  $v(x, y) = 0$ .

Figure 2 shows vorticity past a circular cylinder at  $Re = 100$ . When the steady flow becomes unstable and the body starts shedding vortices, the frequency with which the vortices are shed from the body can be made dimensionless by the formula

$$St = \frac{f_q D}{u_\infty}, \tag{12}$$



Fig. 2. A cycle of vorticity plots past a circular cylinder at  $Re = 100$ ; solid and dotted lines denote negative and positive levels, respectively.

where  $f_q$  is the vortex shedding frequency. The parameter  $St$  is called the Strouhal number. The present Strouhal number at  $Re = 100$  is in reasonable agreement with those of previous numerical and experimental results as shown in Table 2.

#### 4.3. *Moving boundary — Phase-field simulations of dendritic crystal growth in a forced flow*

To show how the present method handles complex moving boundaries, we have conducted simulations of the two-dimensional dendrite growths with and without flow using a phase field model. The phase field variable  $\phi$  is set to be 1 in solid,  $-1$  in melt, and varies smoothly between minus one and plus one in the interface region.

Table 2. The comparison of the numerical and experimental Strouhal number.

<i>Re</i>	Present result	Numerical <sup>a</sup>	Experimental <sup>b</sup>
100	0.1667	0.169	0.16–0.17

<sup>a</sup>[Russell and Wang (2003)]

<sup>b</sup>[Berger and Wille (1972)]

We capture interface by the zero level set of  $\phi$ . The governing equations for dendrite growth with flow as follows [Beckermann *et al.* (1999)]:

$$\frac{\partial \mathbf{u}}{\partial t} + \mathbf{u} \cdot \nabla \mathbf{u} = -\nabla p + Pr \Delta \mathbf{u} + F, \tag{13}$$

$$\nabla \cdot \mathbf{u} = 0, \tag{14}$$

$$\frac{\partial \theta}{\partial t} + D \mathbf{u} \cdot \nabla \theta = D \Delta \theta + \frac{1}{2} \frac{\partial \phi}{\partial t}, \tag{15}$$

$$W(\mathbf{n})^2 \frac{\partial \phi}{\partial t} = [\phi - \lambda \theta (1 - \phi^2)](1 - \phi^2) + \nabla \cdot (W(\mathbf{n})^2 \nabla \phi) + \nabla \cdot \left( |\nabla \phi|^2 W(\mathbf{n}) \frac{\partial W(\mathbf{n})}{\partial \nabla \phi} \right), \tag{16}$$

where  $\theta$  is the rescaled temperature and  $D = 4$  is the dimensionless thermal diffusivity,  $Pr = 23.1$  is the Prandtl number. Following Karma and Rappel [1996], we choose

$$W(\mathbf{n}) = (1 - 3\epsilon_4) \left[ 1 + \frac{4\epsilon_4}{1 - 3\epsilon_4} \frac{\phi_x^4 + \phi_y^4}{|\nabla \phi|^4} \right].$$

The problem parameters are undercooling  $\Delta = -0.55$ ,  $\lambda = 6.383$ , and anisotropy  $\epsilon_4 = 0.05$  (5% anisotropy). In the simulations presented here the initial and inlet melt temperature is  $\theta_{in} = \Delta$ . The initial velocities are taken to be those for steady flow around seed. Equations (13) and (14) are solved using the proposed scheme, while the temperature (15) and the phase-field (16) equations are solved using an explicit method. When we reset the velocity field, we use  $\mathbf{u} = 0.5(1 - \phi)\mathbf{u}$  here.

The computational domain is a square with an initial circular seed. We used a box of  $128 \times 128$ . At the inflow boundary (top) of the computational domain, the uniform velocity and the undercooling temperature are specified. The left and right boundaries are periodic, and the fluid is allowed to flow freely out through the bottom boundary by putting the gradient of temperature and velocity to zero. Results are shown for inlet velocities  $u = 0$ ,  $v = -1$ .  $\Delta t = 0.016$ ,  $\Delta x = 0.8$ .

Figure 3 illustrates the computed evolution of the dendrites without flow (a) and with flow (b). For better visualization, we have interpolated the flow field onto a grid that is about four times coarser than the one used in the computations. It can be seen that the shape of the dendrites is significantly influenced by the flow. The growth rates of the upstream tips are higher than those of the downstream tips

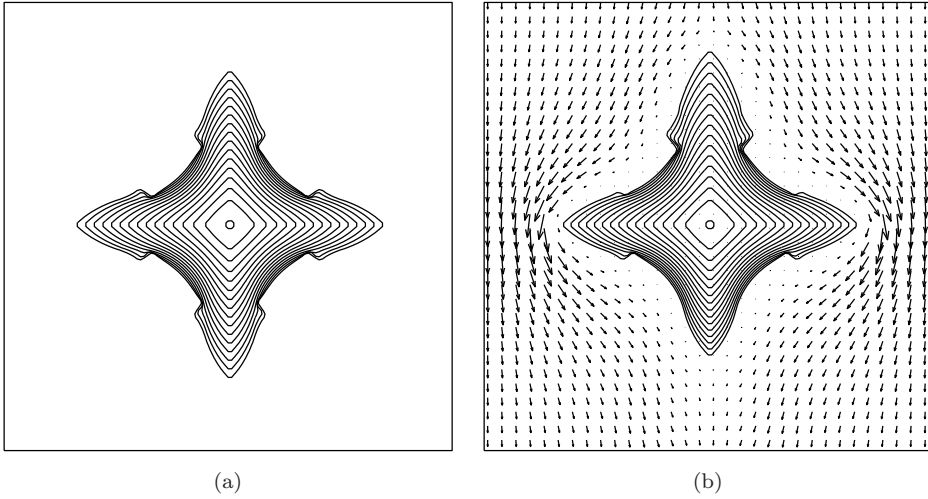


Fig. 3. Evolution of phase-field contours for a dendrite growing at  $\Delta = 0.55$  and  $\epsilon = 0.05$  without convection (a) and with convection (b).

because the impinging flow reduces the thermal boundary-layer thickness on the upstream side. This result is qualitatively in a good agreement with previous result [Beckermann *et al.* (1999)].

#### 4.4. Room ventilation

The flow inside buildings is often the important object of fluid engineering investigations. In this context, a common problem is the effectiveness of room ventilation provided by air conditioning systems in department stores, office buildings, etc. Figure 4 shows the results of the numerical simulation of the ventilation of a model room without (a) and with (b) the augmented projection. Fresh air is introduced through an opening in the top of the domain and one outflow vent is placed in the part of the wall on the right. As it can be seen in the Fig. 4(a), without the augmented projection, the flow field is dissipative and directs toward the objects. However, with the augmented projection Fig. 4(b), the flow field appears to be quite reasonable with the imbedded structure.

### 5. Conclusion

In this paper we have presented an augmented projection method for the incompressible Navier-Stokes equations in an arbitrary moving domain. The projection method has been reformulated and augmented to deal with arbitrary domains. Our numerical examples illustrate that the method is second-order accurate and readily applicable to flows with arbitrarily moving complex immersed boundaries.

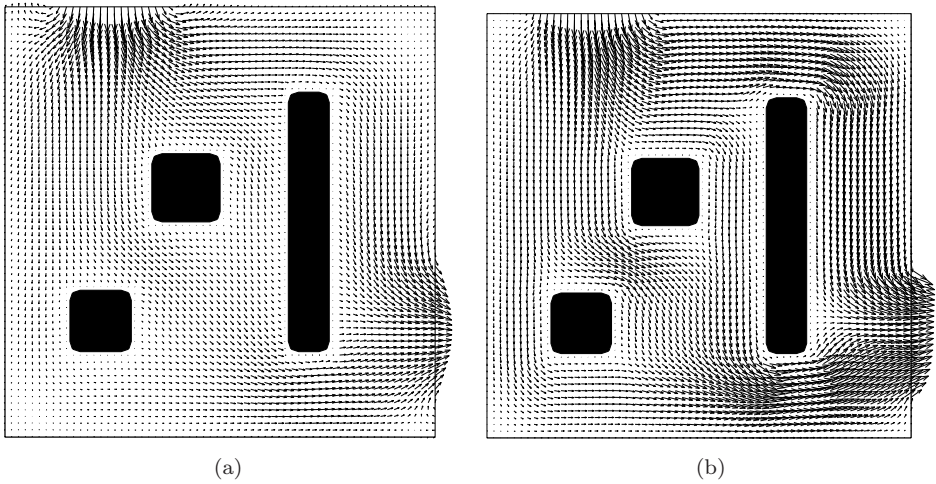


Fig. 4. Numerical results without (a) and with (b) the augmented projection.

Our approach, therefore, should be promising for simulating complex flow/structure interaction problems on Cartesian grids.

### Acknowledgments

The author would like to thank his advisor, John Lowengrub, for the intellectual and financial support. The author acknowledges the support of the National Science Foundation.

### References

- Almgren, A. S., Bell, J. B. and Szymczak, W. G. (1996). A numerical method for the incompressible Navier-Stokes equations based on an approximate projection. *SIAM J. Sci. Comput.*, **17**: 358–369.
- Beckermann, C., Diepers, H. J., Steinbach, I., Karma, A. and Tong, X. (1999). Modeling melt convection in phase-field simulations of solidification. *J. Comput. Phys.*, **154**: 468–496.
- Bell, J., Collela, P. and Glaz, H. (1989). A second-order projection method for the incompressible Navier-Stokes equations. *J. Comput. Phys.*, **85**: 257–283.
- Berger, E. and Wille, R. (1972). Periodic flow phenomena. *Ann. Rev. Fluid Mech.*, **4**: 313–340.
- Fadlun, E. A., Verzicco, R., Orlandi, P. and Mohd-Yusof, J. (2000). Combined immersed-boundary finite-difference methods for three-dimensional complex flow simulations. *J. Comput. Phys.*, **16**: 35–60.
- Johnson, T. and Patel, V. C. (1999). Flow past a sphere up to a Reynolds number of 300. *J. Fluid Mech.*, **378**: 19–70.
- Karma, A. and Rappel, W.-J. (1996). Phase-field method for computationally efficient modeling of solidification with arbitrary interface kinetics. *Phys. Rev. E.*, **53**: 3017–3020.

- Peskin, C. S. (1977). Numerical analysis of blood flow in the heart. *J. Comput. Phys.*, **25**: 220–252.
- Russell, D. and Wang, Z. J. (2003). A Cartesian grid method for modeling multiple moving objects in 2D incompressible viscous flow. *J. Comput. Phys.*, **191**: 177–205.
- Shu, C. W. and Osher, S. (1989). Efficient implementation of essentially non-oscillatory shock capturing schemes II. *J. Comput. Phys.*, **83**: 32–78.
- Strykowski, P. J. and Sreenivasan, K. R. (1990). On the formation and suppression of vortex shedding at low Reynolds numbers. *J. Fluid Mech.*, **218**: 71–107.
- Sussman, M. and Puckett, E. G. (2000). A coupled level set and volume-of-fluid method for computing 3D and axisymmetric incompressible two-phase flows. *J. Comput. Phys.*, **162**: 301–337.
- Tau, E. Y. (1994). A second-order projection method for the incompressible Navier-Stokes equations in arbitrary domains. *J. Comput. Phys.*, **115**: 147–152.
- Udaykumar, H. S., Mittal, R., Rampunggoon, P. and Khanna, A. (2001). A sharp interface Cartesian grid method for simulating flows with complex moving boundaries. *J. Comput. Phys.*, **174**: 345–380.
- Ye, T., Mittal, R., Udaykumar, H. S. and Shyy, W. (1999). An accurate Cartesian grid method for viscous incompressible flows with complex immersed boundaries. *J. Comput. Phys.*, **156**: 209–240.